Available online at www.sciencedirect.com
ScienceDirect
Trans. Nonferrous Met. Soc. China 22(2012) 858−864
Transactions of Nonferrous Metals Society of China
www.tnmsc.cn

# Synthesis and electrochemical properties of $Zn_2SnO_4$ and $Zn_2Sn_{0.8}Ti_{0.2}O_4$/C

YUAN Wan-song, TIAN Yan-wen, LIU Li-juan, LI Jian-zhong

School of Materials and Metallurgy, Northeastern University, Shenyang 110819, China

Received 18 April 2011; accepted 15 June 2011

**Abstract:** Compound $Zn_2Sn_{0.8}Ti_{0.2}O_4$ was synthesized by a hydrothermal method in which $SnCl_4·5H_2O$, $TiCl_4$, $ZnCl_2$ and $N_2H_4·H_2O$ were used as reactants. The composite $Zn_2Sn_{0.8}Ti_{0.2}O_4$/C was then prepared through a carbothermic reduction process using the as-prepared $Zn_2Sn_{0.8}Ti_{0.2}O_4$ and glucose as reactants. The structure, morphology and electrochemical properties of the as-prepared products were investigated by XRD, XPS, TEM and electrochemical measurements. In addition, electrochemical Li insertion/extraction in composite $Zn_2Sn_{0.8}Ti_{0.2}O_4$/C were examined by ex situ XRD and SEM. The first discharge capacity of $Zn_2SnO_4$ is about 1670.8 mA·h/g, with a capacity retain of 342.7 mA·h/g in the 40th cycle at a constant current density of 100 mA/g in the voltage range of 0.05−3.0 V. Comparing with the $Zn_2SnO_4$, some improved electrochemical properties are obtained for $Zn_2Sn_{0.8}Ti_{0.2}O_4$, $Zn_2SnO_4$/C and $Zn_2Sn_{0.8}Ti_{0.2}O_4$/C. The composite $Zn_2Sn_{0.8}Ti_{0.2}O_4$/C shows the best electrochemical properties, and its first discharge capacity is about 1530.0 mA·h/g, with a capacity retain of 479.1 mA·h/g the 100th cycle.
**Key words:** $Zn_2SnO_4$; $Zn_2Sn_{0.8}Ti_{0.2}O_4$/C; titanium substitution; lithium ion batteries; anode materials

## 1 Introduction

The increasing demand for higher energy density and power density of batteries in electronic devices has attracted investigators to develop new materials for lithium-ion batteries. In commercial lithium-ion batteries, graphite is used as an anode material. However, the theoretical capacity of graphite is only 372 mA·h/g [1−3]. Compound $Zn_2SnO_4$ has sparked more interest recently because it can deliver more capacity. When lithium ion inserts into or extracts from it, the following reactions can take place [4−7]:

$$4Li^+ + Zn_2SnO_4 + 4e = Sn + 2Li_2O + 2ZnO \quad (1)$$

$$8Li^+ + Zn_2SnO_4 + 8e = 2Zn + Sn + 4Li_2O \quad (2)$$

$$xLi^+ + Sn + xe = Li_xSn \ (0 \le x \le 4.4) \quad (3)$$

$$yLi^+ + Zn + ye = Li_yZn \ (y \le 1) \quad (4)$$

When lithium ions insert into $Zn_2SnO_4$ particles, they will form metallic Sn and Zn as well as Li−Sn and Li−Zn alloys. It can be seen that about 14.4 lithium ions will react with $Zn_2SnO_4$, Sn and Zn. Based on the above reactions, the theoretical values of irreversible and reversible capacity were calculated to be about 1231 and 547 mA·h/g, respectively. Nevertheless, the most critical problem for $Zn_2SnO_4$ to be used as anode is the severe volume expansion and contraction during the alloying/de-alloying process of the lithium ion with Sn and Zn. Furthermore, metallic Sn and Zn will conglomerate. The large volume change during alloying and de-alloying reactions generates severe stress which results in cracks and crumbling of the particles. This deterioration causes loss of electronic contact between the bulk particles, which gives poor cycle life. To overcome the problem, some improved measures must be taken.

In this study, a hydrothermal method is used to prepare $Zn_2Sn_{0.8}Ti_{0.2}O_4$, and then the as-prepared $Zn_2Sn_{0.8}Ti_{0.2}O_4$ reacts with glucose to produce composite $Zn_2Sn_{0.8}Ti_{0.2}O_4$/C. To our best knowledge, the electrochemical features of composite $Zn_2Sn_{0.8}Ti_{0.2}O_4$/C are rarely reported.

## 2 Experimental

### 2.1 Synthesis procedure

The pure $Zn_2SnO_4$ was synthesized by hydrothermal reaction at 180 °C according to the method previously reported by YUAN et al [7]. The $Zn_2Sn_{0.8}Ti_{0.2}O_4$ was

**Foundation item:** Project (51004028) supported by the National Natural Science Foundation of China
**Corresponding author:** TIAN Yan-wen; Tel: +86-24-83684943; E-mail: yuanwansong2010@163.com
DOI: 10.1016/S1003-6326(11)61257-0

also synthesized by hydrothermal reaction under the same conditions as synthesis of $Zn_2SnO_4$. In this process, analytical grade reagents $SnCl_4·5H_2O$, $TiCl_4$, $ZnCl_2$ and $N_2H_4·H_2O$ were used as reactants. The molar ratio of Zn to Sn to Ti to $N_2H_4·H_2O$ was 2:0.8:0.2:8. Zinc chloride, tin chloride, and titanium chloride were dissolved into distilled water to form transparent solution under magnetic stirring. $N_2H_4·H_2O$ was then added dropwise into the mixture to form white slurry. After stirring for 30 min, the final mixture was transferred into a Teflon-lines stainless steel autoclave with a filling capacity of 80%. The autoclave was maintained at 180 °C for 24 h, and cooled naturally to room temperature. The precipitate was filtered and washed with ethanol and deionized water several times. Finally, the product was dried at 80 °C for 12 h.

After $Zn_2SnO_4$ and $Zn_2Sn_{0.8}Ti_{0.2}O_4$ were obtained, the composites $Zn_2SnO_4$/C and $Zn_2Sn_{0.8}Ti_{0.2}O_4$/C were then prepared through a carbothermic reduction process, respectively. The as-prepared $Zn_2SnO_4$ and $Zn_2Sn_{0.8}Ti_{0.2}O_4$ were separately mixed with glucose ($C_6H_{12}O_6$) together at a mass ratio of 85:15. This mixture was put into distilled water under magnetic stirring, and then dried at 80 °C. At last, the dried mixtures were separately calcined at 600 °C for 2 h under Ar atmosphere to obtain composite $Zn_2SnO_4$/C and $Zn_2Sn_{0.8}Ti_{0.2}O_4$/C.

### 2.2 Analysis of active materials

The prepared samples were identified and characterized on a X-ray powder diffractometer (Rigaku Co. Ltd). X-ray profiles were measured between 10° and 80° (2$\theta$ angle) with a monochromatic Cu $K_\alpha$ radiation source. Transmission electron microscopy (TEM, FEI Tecnai 12) was also employed to characterize the as-prepared samples. X-ray photoelectron spectra (XPS) were measured at room temperature on an ESCALAB 250. During XPS analysis, the Al $K_\alpha$ X-ray beam was adopted as the excitation source, and the power was set to be 150 W. Vacuum pressure of the instrument chamber was $1\times10^{-7}$ Pa read on the panel. In addition, SEM was also used to observe the change of electrodes in morphology and microstructure before and after given cycles.

### 2.3 Electrochemical test

In order to evaluate the electrochemical characteristics, the working electrode was prepared by pressing a mixture of the active material, conducting carbon black, and binder (PVDF) in a mass ratio of 70:15:15. Li foil was used as the counter and reference electrodes. The electrolyte was 1 mol/L $LiPF_6$ in a mixture of ethylene carbonate (EC), diethyl carbonate (DMC), ethylene methyl carbonate (EMC) with a volume ratio of 1:1:1. The cells were assembled in an argon-filled dry box. Charge-discharge tests were performed in the voltage range of 0.05−3.0 V at the current density of 100 mA/g.

## 3 Results and discussion

### 3.1 Structure characterization of materials

$Zn_2SnO_4$ belongs to the inverse spinel structure where the tetrahedral voids are occupied by the Zn atoms and the octahedral voids are occupied by equal number of Zn and Sn atoms [8]. X-ray diffraction patterns of the $Zn_2SnO_4$, $Zn_2Sn_{0.8}Ti_{0.2}O_4$, $Zn_2SnO_4$/C and $Zn_2Sn_{0.8}Ti_{0.2}O_4$/C are shown in Fig. 1. It is clearly seen that all diffraction peaks of the four samples are agree well with the reverse spinel structure of $Zn_2SnO_4$ (JCPDS, Card No. 24—1470), suggesting that these materials prepared under our conditions are well-crystallized and partial substitution of Ti for Sn in the $Zn_2SnO_4$ will not change the crystal structure. Figure 1 also reveals that some diffraction peaks of the samples with Ti-doping undergo a slight shift toward higher degrees. For clear observation, the peak position of (440) planes of $Zn_2SnO_4$ and $Zn_2Sn_{0.8}Ti_{0.2}O_4$ are magnified and shown in Fig. 2. In addition, the diffraction peak intensities of $Zn_2SnO_4$ and $Zn_2Sn_{0.8}Ti_{0.2}O_4$/C are stronger than that of the $Zn_2SnO_4$ because they were heat-treated at 600 °C.

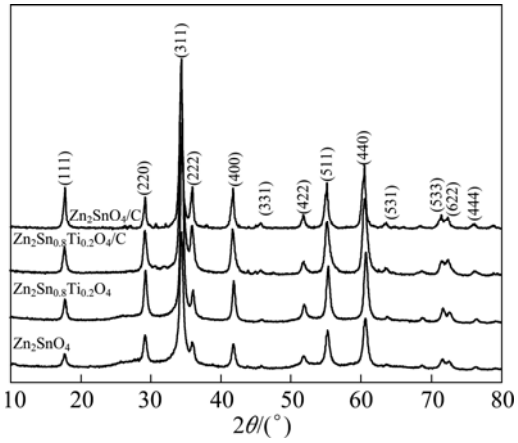


**Fig. 1** XRD patterns of $Zn_2SnO_4$, $Zn_2Sn_{0.8}Ti_{0.2}O_4$ and $Zn_2SnO_4$/C and $Zn_2Sn_{0.8}Ti_{0.2}O_4$/C

The lattice parameters for $Zn_2SnO_4$ and $Zn_2Sn_{0.8}Ti_{0.2}O_4$ samples were calculated by least square fitting as 8.6550 Å and 8.6452 Å based on the XRD peaks, respectively, which were in accordance with the standard XRD data (JCPDS, Card No. 24—1470). The chemical valences of Ti, Sn and Zn in the $Zn_2Sn_{0.8}Ti_{0.2}O_4$ are +4, +4 and +2, respectively. The ionic radii of $Ti^{4+}$,

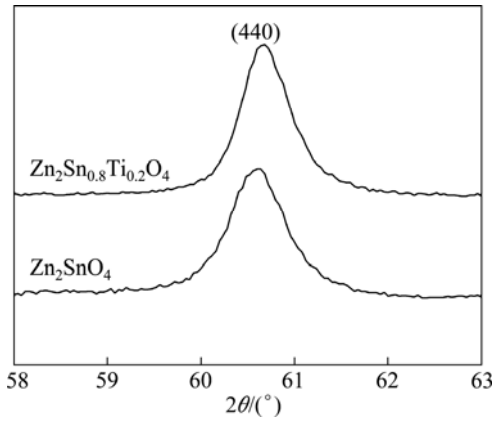


**Fig. 2** Enlarged (440) peaks of $Zn_2SnO_4$ and $Zn_2Sn_{0.8}Ti_{0.2}O_4$ in Fig. 1

$Sn^{4+}$ and $Zn^{2+}$ are 0.61 Å, 0.71 Å and 0.74 Å, respectively. Because the ionic radius of $Ti^{4+}$ is smaller than that of Sn, which is substituted for the lattice constant of $Zn_2Sn_{0.8}Ti_{0.2}O_4$ is smaller than that of $Zn_2SnO_4$.

It is well known that the X-ray photoelectron spectrum (XPS) is an effective tool for the study of material surface and to investigate the chemical state of elements in compound. Figure 3 presents XPS of the $Zn_2SnO_4$ and $Zn_2Sn_{0.8}Ti_{0.2}O_4$. The peaks in the $Zn_2SnO_4$, Zn 2p (1021.79 eV), Sn 3d (486.0 eV) and O1s (530.3 eV) are detected. The peaks of the Zn 2p and Sn 3d spectra for the Ti-doping material almost have no inspective change on the binding energy, compared with $Zn_2SnO_4$, indicating that the Zn and Sn ion environments in the structure were not changed after doping Ti. Meanwhile, the XPS spectrum of Ti is shown in Fig. 3(d). The XPS spectrum of Ti $2p_{3/2}$ shows the characteristic peaks at 458.62 eV, which is similar to the binding energies of $Ti^{4+}$ in $TiO_2$ [9].

### 3.2 Morphology of materials

Figures 4 (a) and (b) display TEM images of the as-prepared $Zn_2SnO_4$ and composite $Zn_2Sn_{0.8}Ti_{0.2}O_4$/C samples, respectively. It can be seen that $Zn_2SnO_4$ particles have irregular shapes and consist of a number of small crystallites with a diameter between 20 and 30 nm. Composite $Zn_2Sn_{0.8}Ti_{0.2}O_4$/C particles also exhibit irregular shapes but the particle size is a bit larger.

### 3.3 Electrochemical performance and changes of electrode structure and morphology

The charge−discharge curves of $Zn_2SnO_4$ and composite $Zn_2Sn_{0.8}Ti_{0.2}O_4$/C are shown in Fig. 5. For

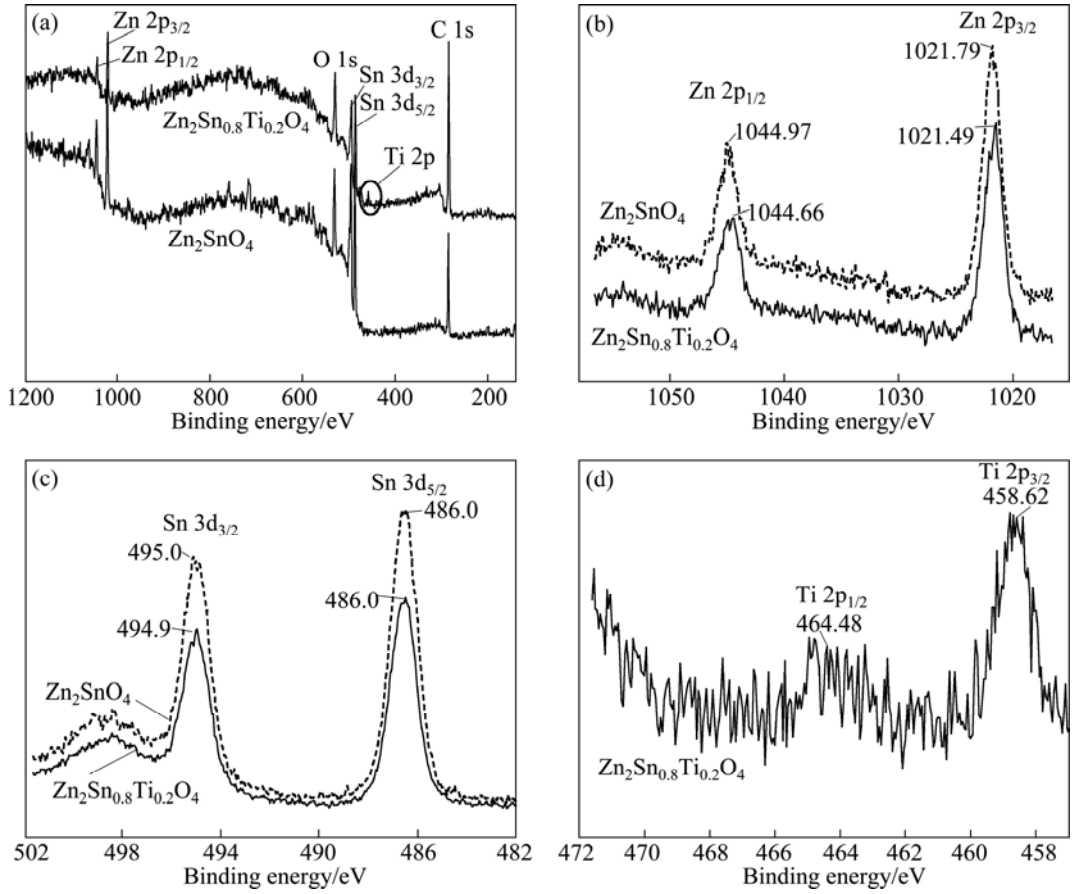


**Fig. 3** XPS spectra of pure phase $Zn_2SnO_4$ and $Zn_2Sn_{0.8}Ti_{0.2}O_4$ (a), Zn (b), Sn (c) and Ti (d)

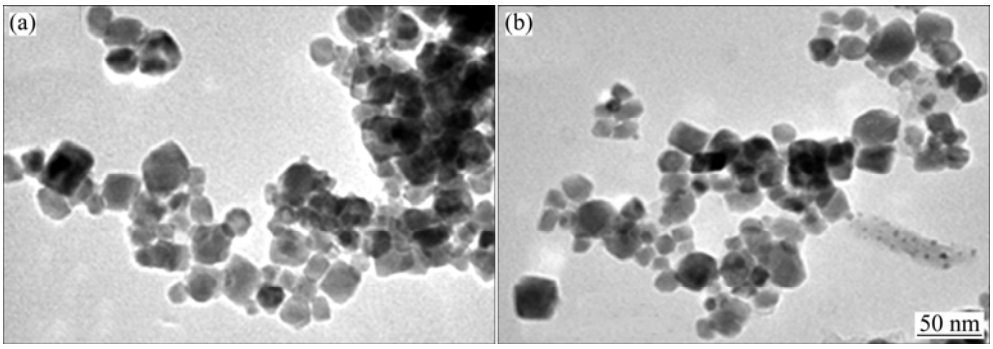


**Fig. 4** TEM images of $Zn_2SnO_4$ (a) and composite $Zn_2Sn_{0.8}Ti_{0.2}O_4$/C (b)

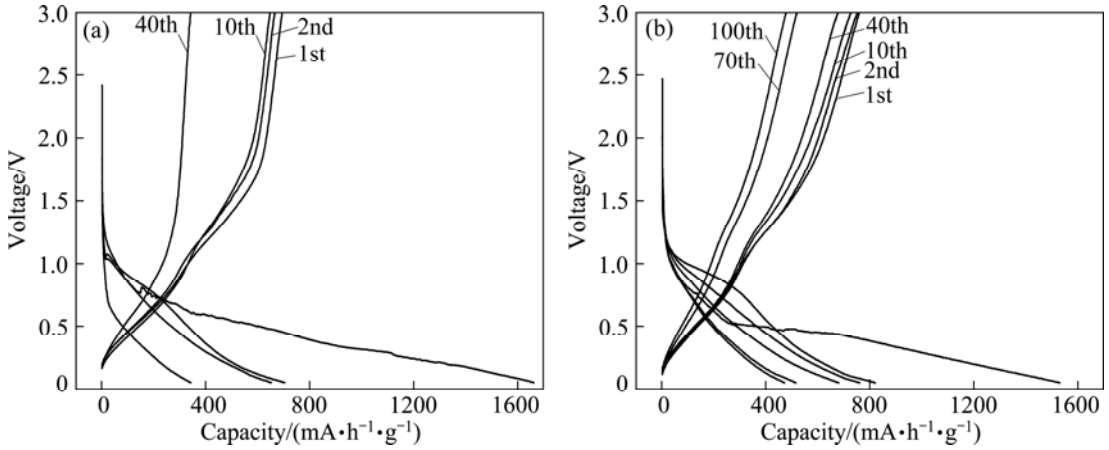


**Fig. 5** Charge−discharge curves of product: (a) $Zn_2SnO_4$; (b) Composite $Zn_2Sn_{0.8}Ti_{0.2}O_4$/C

$Zn_2SnO_4$, its first discharge and charge capacities are about 1670.8 and 689.5 mA·h/g, respectively. The irreversible capacity in the first discharge is up to 981.3 mA·h/g, which is different from the subsequent discharge. Based on Eq. (1) to Eq. (4), the theoretical capacity derived from the maximum uptake of 14.4 Li/$Zn_2SnO_4$ is about 1231 mA·h/g, which is smaller than that of the initial discharge. This is probably caused by the formation of a solid electrolyte interphase (SEI) film [10]. The large irreversible discharge capacity after the first cycle is probably due to severe side reaction with the electrolyte to form $Li_2O$ and SEI film, especially for the nano-$Zn_2SnO_4$ particles with the smaller size and larger surface area. There is almost no capacity above the 1.0 V in the first discharge curve and a wide platform at 1.0−0.5 V can be observed. However, from the second cycle afterward, all the potential plateaus are very similar and display more inclined shape. An obvious result is that the plateau in the first cycle disappears in the subsequent cycles owing to the change of the active electrode material after the first cycle. To further confirm the electrode change in structure, the XRD patterns of the $Zn_2SnO_4$ material and the $Zn_2SnO_4$ specimen taken from the electrode at the charged state and discharged state after one cycle are presented in Fig. 6.

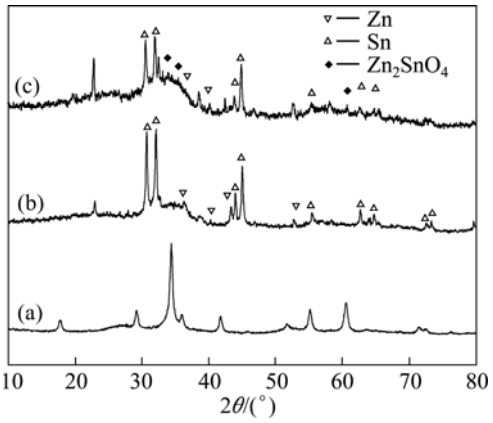


**Fig. 6** XRD patterns of $Zn_2SnO_4$ electrode before and after the first charge−discharge: (a) Initial state; (b) At discharge state; (c) At charge state

Three phases, inversed spinel $Zn_2SnO_4$, Zn and Sn, are detected at the charged state. It is found that most Li−Sn and Li−Zn alloys can be reversibly decomposed. In the case of the discharged state, the diffraction peaks of inversed spinel $Zn_2SnO_4$ disappear, but Zn and Sn exist. This proves that in the discharge process the $Zn_2SnO_4$ particles are reduced to Zn and Sn. Meanwhile, amorphous $Li_2O$ as well as Li−Sn and Li−Zn alloys are

also generated. There is an obvious tendency for capacity to reduce. For example, the charge capacities in the 2nd, 10th and 40th cycle are 694.9, 648.3 and 342.7 mA·h/g, respectively. Its capacity retention is only 49.3% of the first charge capacity after 40 cycles.

The first discharge and charge capacities of the composite $Zn_2Sn_{0.8}Ti_{0.2}O_4$/C electrode are 1530.0 and 752.3 mA·h/g, respectively. The composite $Zn_2Sn_{0.8}Ti_{0.2}O_4$/C electrode shows an initial columbic efficiency of approximately 49.2%, which is higher than that of $Zn_2SnO_4$ (41.8%). From the second cycle, the columbic efficiency increases to more than 90%. It is considered that this should behave in a similar electrochemically manner to $Zn_2SnO_4$, although the products are slightly different.

XRD is also applied to analyzing the composite $Zn_2Sn_{0.8}Ti_{0.2}O_4$/C electrode change in structure. The XRD pattern of the composite $Zn_2Sn_{0.8}Ti_{0.2}O_4$/C specimen taken from the electrode at the charged state and discharged state after one cycle is presented in Fig. 7. Four phases, inversed spinel $Zn_2SnO_4$, Zn, Sn and $TiO_2$ are detected at the charged state. It is found that most

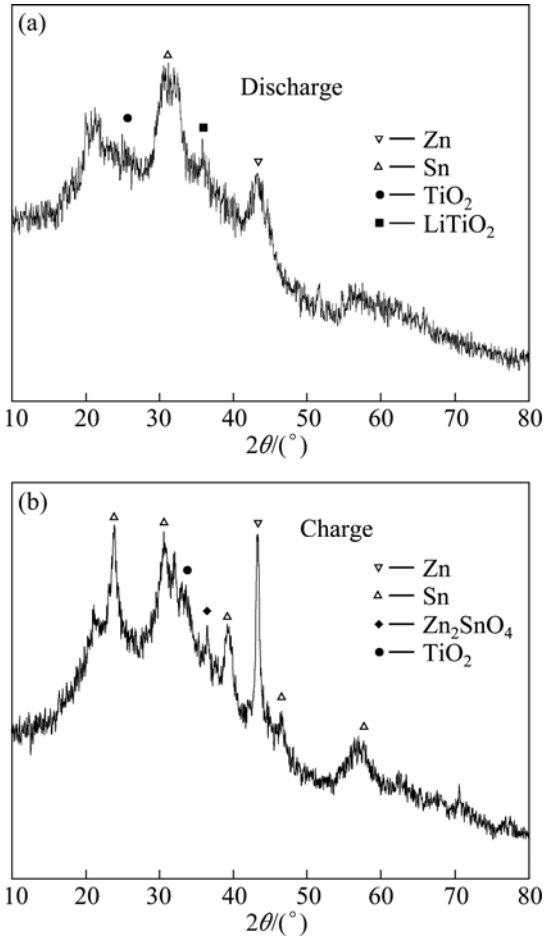


**Fig. 7** XRD patterns of composite $Zn_2Sn_{0.8}Ti_{0.2}O_4$/C electrode after the first charge−discharge: (a) At discharge state; (b) At charge state

Li−Sn and Li−Zn alloys can be reversibly decomposed. In the case of the discharged state, the diffraction peaks of inversed spinel $Zn_2SnO_4$ disappear, but Zn and Sn exist. This proves that in the discharge process the composite $Zn_2Sn_{0.8}Ti_{0.2}O_4$/C particles are also reduced to Zn and Sn as $Zn_2SnO_4$. Meanwhile, $TiO_2$ and $LiTiO_2$ are also detected.

For titania, the lithium insertion / extraction to $TiO_2$ proceeds according to the following reversible reaction: $TiO_2+xLi^++xe=Li_xTiO_2$. The maximum $x$ for the reversible reaction of normal crystalline anatase $TiO_2$ is 0.5, which corresponds to a capacity of 168 mA·h/g [11]. During the insertion process, the crystal structure of $Li_xTiO_2$ changes from tetragonal $Li_{0.05}TiO_2$ to orthorhombic $Li_{0.5}TiO_2$, but it can maintain the structure stability during the charge−discharge process [12]. Moreover, the active $TiO_2$ and inactive $LiTiO_2$ are useful for enhancing the mechanical properties of the matrix by alleviating the volume expansion/contraction of active (Sn, Zn) nanocrystallites, which occurs during cycling within a nanostructure composite [13−15].

The cycling behaviors of $Zn_2SnO_4$, $Zn_2Sn_{0.8}Ti_{0.2}O_4$, $Zn_2SnO_4$/C and $Zn_2Sn_{0.8}Ti_{0.2}O_4$/C electrodes are shown in Fig. 8. Although the $Zn_2SnO_4$ electrode delivers very high initial discharge capacity, its capacity retention is quite poor. The $Zn_2Sn_{0.8}Ti_{0.2}O_4$, $Zn_2SnO_4$/C and $Zn_2Sn_{0.8}Ti_{0.2}O_4$/C electrodes deliver an initial discharge capacity of 1548.4, 1512.7 and 1530.0 mA·h/g, respectively, which are just a bit lower than that of $Zn_2SnO_4$ electrode. However, they show much better capacity retention than $Zn_2SnO_4$ electrode. After 40 cycles, the charge capacity of $Zn_2Sn_{0.8}Ti_{0.2}O_4$, composites $Zn_2SnO_4$/C and $Zn_2Sn_{0.8}Ti_{0.2}O_4$/C remain at 413.4, 500.1 and 674.5 mA·h/g, respectively. The capacity retentions of $Zn_2Sn_{0.8}Ti_{0.2}O_4$, $Zn_2SnO_4$/C and $Zn_2Sn_{0.8}Ti_{0.2}O_4$/C are 72.5%, 51.9% and 89.6%, respectively. Obviously, the capacity retention of the

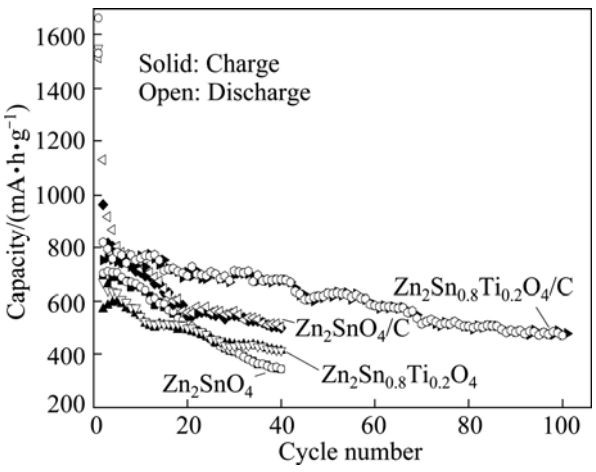


**Fig. 8** Cycling performance of products

$Zn_2Sn_{0.8}Ti_{0.2}O_4$/C is excellent compared with $Zn_2Sn_{0.8}Ti_{0.2}O_4$ and $Zn_2SnO_4$/C electrodes. It suggests that a synergistic effect may exist between Ti element in this composite and carbon matrix during cycling. The $Zn_2Sn_{0.8}Ti_{0.2}O_4$/C electrode shows a very stable capacity of 479.1 mA·h/g over 100 cycles, which is even much higher than the theoretical capacity of graphite. From the first to the 100th cycle, the charge capacity for $Zn_2Sn_{0.8}Ti_{0.2}O_4$/C decreases from 752.3 to 497.1 mA·h/g, with a little average capacity fading of 2.5 mA·h/g per cycle, which shows the best capacity retention of this material advanced so far [4−7]. The improvement of electrochemical behavior should be attributed to the unique composite structure consisting of active Zn, Sn and $TiO_2$, and inactive $LiTiO_2$ in the carbon matrix. Firstly, the amorphous carbon in composite can dissociate the metallic Sn and Zn particles and improve a high electrical conductivity for composites. Secondly, the $TiO_2$ itself is electroactive material for lithium storage and contributes to overall capacity of electrodes. Thirdly, the active $TiO_2$ and inactive $LiTiO_2$ can not only enhance mechanical properties of the matrix to accommodate the stress generated during cycling, but also dissociate the metal Sn and Zn particles.

In order to shed the light on the enhanced electrochemical performance of material via doping, the morphological changes of the composite electrodes after different cycles were examined by SEM (Fig. 9). After 20 cycles, severe agglomeration appears in the $Zn_2SnO_4$ electrode, while there is no significant change in microstructure of $Zn_2Sn_{0.8}Ti_{0.2}O_4$/C electrode. This indicates that the amorphous carbon, the active $TiO_2$ and inactive $LiTiO_2$ can dissociate the metallic Sn and Zn particles, and the degree of Sn and Zn particles conglomerate can be decreased. The present results agree well with the above analysis.

## 4 Conclusions

1) The composite $Zn_2Sn_{0.8}Ti_{0.2}O_4$/C was synthesized by a hydrothermal method and subsequent carbothermic reduction process. The structure, morphology and electrochemical properties of $Zn_2Sn_{0.8}Ti_{0.2}O_4$/C were investigated by XRD, XPS, TEM and electrochemical measurements.

2) The XRD and XPS results show that Ti is indeed incorporated into the $Zn_2SnO_4$ crystal structure.

3) The composite $Zn_2Sn_{0.8}Ti_{0.2}O_4$/C shows a better electrochemical performance than most previously reported $Zn_2SnO_4$ samples, with a much higher capacity of 479.1 mA·h/g after 100 cycles.

4) The larger capacity and better cyclability of the composite $Zn_2Sn_{0.8}Ti_{0.2}O_4$/C electrode are attributed to composite structure consisting of active Zn, Sn and $TiO_2$, and inactive $LiTiO_2$ in the carbon matrix during the cycling process.

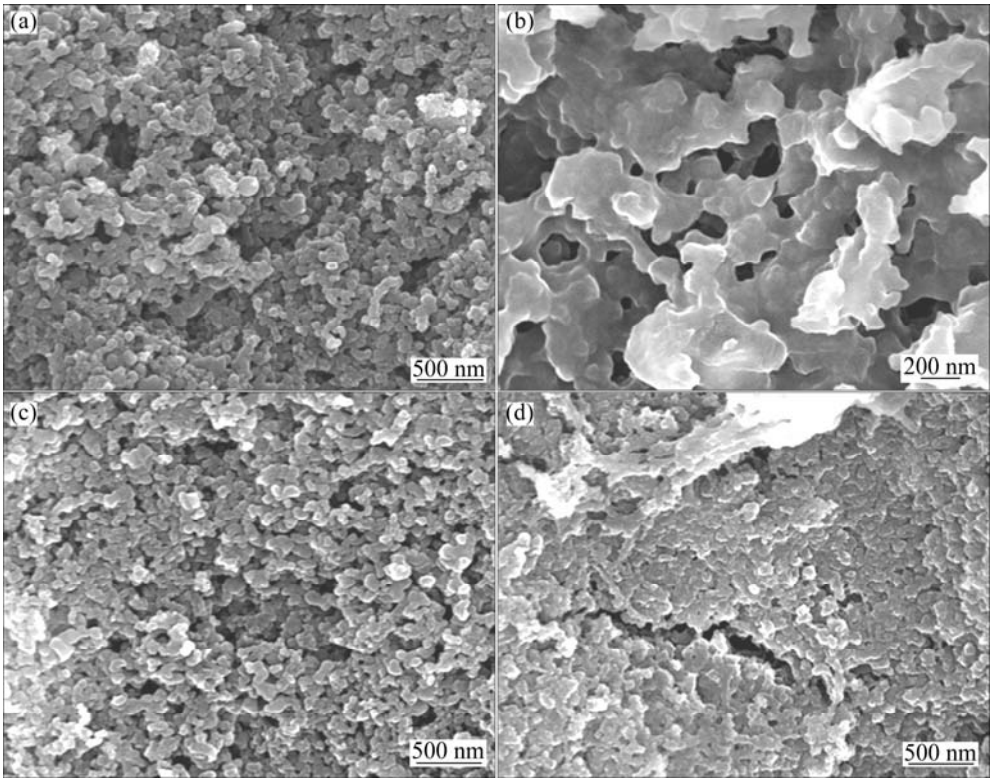


**Fig. 9** SEM images of $Zn_2SnO_4$ electrode (a, b) and $Zn_2Sn_{0.8}Ti_{0.2}O_4$/C electrode (c, d): (a), (c) Before cycle; (b), (d) After 20 cycles

## References


[1] WU Y P, JIANG C, WU C, HOLZE R. Anode materials for lithium ion batteries by oxidative treatment of common natural graphite [J]. Solid State Ionics, 2003, 156(3−4): 283−290.

[2] BUKKAYD D, NABAIS C, MERCIER C, SCHNEIDER R, WILLMANN P. Electrochemical lithium insertion in graphite containing dispersed tin–antimony alloys [J]. Energy Convers Manage, 2008, 49: 2447−2454.

[3] HUGGINS R A. Alternative materials for negative electrodes in lithium systems [J]. Solid State Ionics, 2002, 152−153: 61−68.

[4] RONG A, GAO X P, LI G R, YAN T Y, ZHU H Y, QU J Q, SONG D Y. Hydrothermal synthesis of $Zn_2SnO_4$ as anode materials for Li-ion battery [J]. J Phys Chem B, 2006, 110: 14754−14760.

[5] ZHU X J, GENG L M, ZHANG F Q, LIU Y X, CHENG L B. Synthesis and performance of $Zn_2SnO_4$ as anode materials for lithium ion batteries by hydrothermal method [J]. J Power Sources, 2009, 189(1): 828−831.

[6] HOU X G, CHENG Q, BAI Y, ZHANG W F. Preparation and electrochemical characterization of $Zn_2SnO_4$ as anode materials for lithium ion batteries [J]. Solid State Ionics, 2010, 181(3−4): 631−634.

[7] YUAN W S, TIAN Y W, LIU G Q. Synthesis and electrochemical properties of pure phase $Zn_2SnO_4$ and composite $Zn_2SnO_4$/C[J]. J Alloys Compd, 2010, 506: 683−687.

[8] FU Z L, YANG H K, MOON B K, CHOI B C, JEONG J H. Hydrothermal synthesis and optical characteristics of $Eu^{3+}$ in $Zn_2SnO_4$ nanocrystals [J]. Current Applied Physics, 2009, 9: 1360−1364.

[9] HAO Y J, LAI Q Y, LIU D Q, XU Z U, JI X Y. Synthesis by citric acid sol–gel method and electrochemical properties of $Li_4Ti_5O_{12}$ anode material for lithium-ion battery [J]. Mater Chem Phys, 2005, 94(2−3): 382−387.

[10] XIAO T, TANG Y W, JIA Z Y, FENG S L. Synthesis of $SnO_2$/$Mg_2SnO_4$ nanoparticles and their electrochemical performance for use in Li-ion battery electrodes [J]. Electrochim Acta, 2009, 54(8): 2396−2401.

[11] LINDSTROM H, SODERGREN S, SOLBRAND A, RENSMO H, HJELM J, HAGFELDT A, LINDQUIST S E. $Li^+$ ion insertion in $TiO_2$ (anatase): 1. Chronoamperometry on CVD films and nanoporous films [J]. J Phys Chem B, 1997, 101(39): 7710−7716.

[12] ZHAO Z W, GUO Z P, WEXLER D, MA Z F, XU X, LIU H L. Titania nanotube supported tin anodes for lithium intercalation [J]. Electrochem Commun, 2007, 9(4): 697−702.

[13] PARK C M, CHANG W S, JUNG H, KIM J H, SOHN H J. Nanostructured Sn/$TiO_2$/C composite as a high-performance anode for Li-ion batteries [J]. Electrochem Commun, 2009, 11: 2165−2168.

[14] JEONG G J, KIM Y U, SOHN H J, KANG T. Particulate-reinforced Al-based composite material for anode in lithium secondary batteries [J]. J Power Sources, 2001, 101(2): 201−205.

[15] MAO O, TURNER R L, COURTNEY I A, FREDERICKSEN B D, BUCKETT M I, KRAUSE L J, DAHN J R. Electrochem active/inactive nanocomposites as anodes for Li-ion batteries [J]. Solid-State Lett, 1999, 2(1): 3−5.


# $Zn_2SnO_4$ 和 $Zn_2Sn_{0.8}Ti_{0.2}O_4$/C 的制备和电化学性能


袁万颂，田彦文，刘丽娟，李建中

东北大学 材料与冶金学院，沈阳 110819



**摘 要**：以 $SnCl_4·5H_2O$、$TiCl_4$、$ZnCl_2$ 和 $N_2H_4·H_2O$ 为原料，采用水热法制备 $Zn_2Sn_{0.8}Ti_{0.2}O_4$ 纳米粉体。在此基础上，以葡萄糖和水热合成的 $Zn_2Sn_{0.8}Ti_{0.2}O_4$ 为原料，以碳热还原法制备 $Zn_2Sn_{0.8}Ti_{0.2}O_4$/C 复合材料。利用 XRD、XPS、TEM、恒电流充放电等方法分别研究 $Zn_2SnO_4$ 和 $Zn_2Sn_{0.8}Ti_{0.2}O_4$/C 复合材料的结构、形貌和电化学性能。同时用非原位 XRD、XPS 和 SEM 分析 $Zn_2Sn_{0.8}Ti_{0.2}O_4$/C 复合材料电极在充放电过程中的结构和形貌变化。合成的纯 $Zn_2SnO_4$ 的首次放电容量为 1670.8 mA·h/g，循环 40 次后放电容量迅速衰减为 342.7 mA·h/g。而 $Zn_2Sn_{0.8}Ti_{0.2}O_4$/C 复合材料的首次放电容量为 1530.0 mA·h/g，循环 100 次后容量还保持为 479.1 mA·h/g，与纯 $Zn_2SnO_4$、$Zn_2Sn_{0.8}Ti_{0.2}O_4$ 和 $Zn_2SnO_4$/C 相比，电化学性能有较大的提高。



**关键词**：$Zn_2SnO_4$；$Zn_2Sn_{0.8}Ti_{0.2}O_4$/C；钛掺杂；锂离子电池；负极材料

**(Edited by LI Xiang-qun)**